OPEN ACCESS

University of BRISTOL

Conceicao, R., Byrne, D., Ghavami, N., Probert Smith, P., & Craddock, I. (2015). Spectral filtering in phase delay beamforming for multistatic UWB breast cancer imaging. In 2015 9th European Conference on Antennas and Propagation (EuCAP 2015): Proceedings of a meeting held 13-17 April 2015, Lisbon, Portugal. (pp. 1-4). (Proceedings of the European Conference on Antennas and Propagation). Institute of Electrical and Electronics Engineers (IEEE).

Peer reviewed version

Link to publication record in Explore Bristol Research
PDF-document

Spectral Filtering in Phase Delay Beamforming for Multistatic UWB Breast Cancer Imaging

Raquel C. Conceição[1], Dallan Byrne[2], Navid Ghavami[3], Penny Probert Smith[4], Ian Craddock[2]

[1] Institute of Biomedical Engineering, University of Oxford, Headington, Oxford OX3 7DQ, UK; Instituto de Biofísica e Engenharia Biomédica, Faculdade de Ciências, Universidade de Lisboa, Portugal; raquelcruzconceicao@gmail.com

[2] Department of Electrical & Electronic Engineering, University of Bristol, UK

[3] Institute of Biomedical Engineering, University of Oxford, Headington, Oxford OX3 7DQ, UK

[4] Lady Margaret Hall, University of Oxford, UK

Abstract—In this paper, the authors propose the use of spectral beamforming for the reconstruction of a breast energy profile for cancer detection. Experiments were performed on three different breast phantoms and different spectral beamformers were implemented and tested.

Index Terms—Breast Microwave Imaging, Spectral Beamforming.

I. INTRODUCTION

Microwave Imaging has been extensively studied in the context of breast imaging for almost two decades. Radar Ultra Wideband (UWB) imaging techniques have been largely examined for monostatic (e.g. [1]) and multistatic antenna configurations (e.g. [2]). Different authors have proposed different imaging algorithms to remove the large artefact caused by the skin on the breast surface, and several beamformers have been proposed to detect dielectric scatterers (*e.g.* tumours) within the breast.

Most existing Microwave Imaging prototypes designed for breast imaging have reported the use of Vector Network Analysers (VNAs) to illuminate the breast phantoms and also record the resulting backscattered signals. As a natural consequence, all these signals are produced and recorded in the Frequency Domain (FD). However, most reported imaging algorithms, such as skin artefact removals and beamformers, are often reported in the Time Domain (TD). This implies that signals are first converted to TD through an Inverse Fast Fourier Transform before having subjected through a skin artefact removal algorithm and a beamformer – which often involves time-consuming multiplication and summation of large matrices.

In this paper, the authors will present FD algorithms to remove the skin artefact and beamform the backscattered signals of three different breast phantoms with a tumour model.

II. MATERIALS

A. Microwave Imaging System Description

The Microwave Imaging system used in this study comprises a Rohde-Shwarz ZVT 8 port VNA – operating in the 4-8GHz frequency range – and a conformal array of 60 wide-slot antennas [2]. The antennas operate while immersed in a matching liquid. E_{nm} is the measured backscattered signal received at receiving antenna *m* from transmitting antenna *n*. A low-loss matching ceramic shell is then fitted into the antenna array, into which the breast phantoms will be placed. To note that the antenna array was rotated by 10 degrees to provide differential measurements, which are used for the skin calibration method.

B. Phantoms

Three breast phantoms were developed, and tested three times. Breast phantom I reflects a homogeneous breast phantom with an evenly distributed layer of skin with a thickness varying between 1 and 3 mm, a tumour phantom was placed at $(-20, -20, -25)$ location. The interior of the phantom is then filled with homogeneous matching liquid which aims to exhibits similar dielectric properties to the internal breast tissue.

Breast phantom II comprises a layer of skin with thickness varying between 1 and 3 mm, a piece of Tissue Mimicking Material (TMM) – to account for some breast heterogeneity – placed at $(20,20,-12)$, a tumour phantom placed at $(-20, -20, -20)$ and the interior is filled with matching liquid.

Breast phantom III (Fig. 1) also comprises a layer of skin with thickness varying between 1 and 3 mm, a piece of tissue mimicking material placed at $(0, -30, -10)$, a tumour phantom
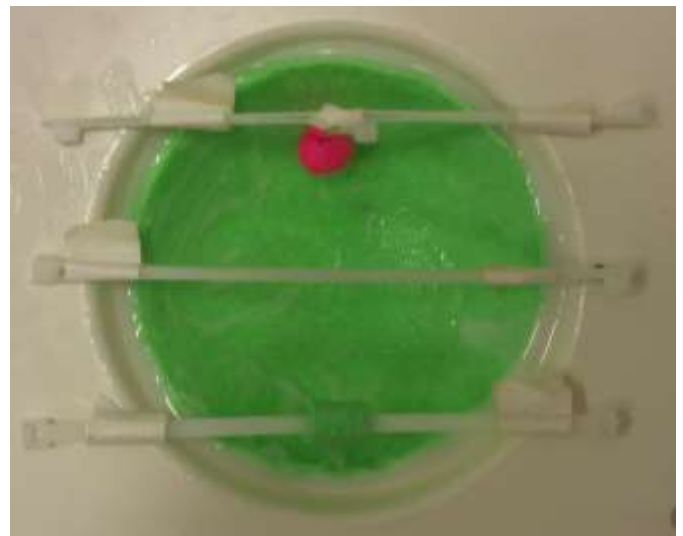

Fig. 1. Breast phantom III with skin, tumour and fibroglandular mimicking marterlials before filled with matching liquid.

placed at $(0, 20, -15)$ and the interior is then filled with matching liquid.

For all breast phantoms, the chest-wall was accounted for by maintaining a liquid to air interface at the base of the breast phantom. The dielectric properties at 6 GHz for the skin TMM were $\varepsilon_r = 30$, $\sigma = 4\ s/m$ for Phantom I, and $\varepsilon_r = 33$, $\sigma = 3.9\ s/m$ for Phantoms II and III. The matching liquid had $\varepsilon_r = 9.3$, $\sigma = 0.22\ s/m$. The tumour TMM had the following dielectric properties: $\varepsilon_r = 50$, $\sigma = 7\ s/m$. The heterogeneous breast TMM had the following dielectric properties: $\varepsilon_r = 30$, $\sigma = 3.9\ s/m$ for Phantoms II and III.

III. IMAGE RECONSTRUCTION

Two algorithms are often needed for the reconstruction of the energy profile of the breast: skin artefact removal algorithm and beamforming algorithm.

A. Skin Artefact Removal Algorithms

An artefact removal algorithm is applied to the recorded signals to subtract the high backscattering response caused by skin. The large skin artefact is caused by the large dielectric difference between the skin and the normal breast tissue which causes a large reflection in the recorded backscattered data, and also by a creep wave which propagates between nearby antennas without entering the phantom. A simple but effective method to reduce this effect involves taking two sets of data displaced by a small angle of rotation, $\theta_{rot} = 10°$. The skin signal may be assumed to be unaffected by the rotation whereas internal reflections are displaced. By subtracting the two sets of measurements, E_{nm1} and E_{nm2}, so that:

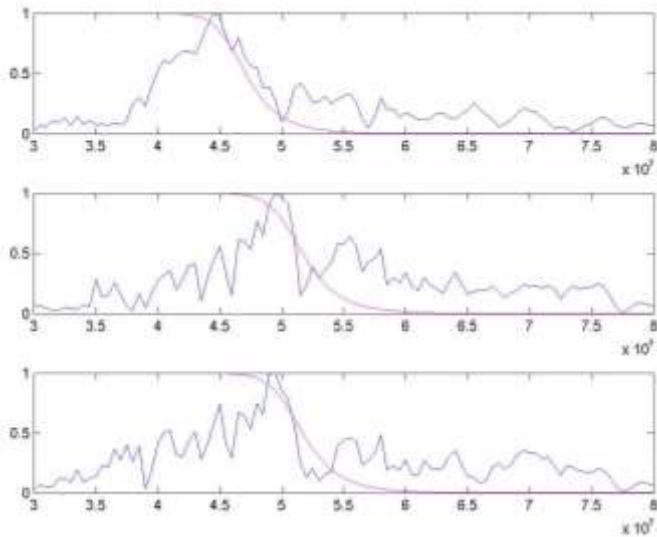$$E_{nm} = E_{nm1} - E_{nm2} \qquad (1)$$

Fig. 2. The spectrum of the zero mean signal over all the antenna paths in blue. Breast phantoms I, II and III (from top to bottom). The response of a 20th order Butterworth filter with -3dB frequency are shown in purple (with cut-off frequency of 4.5 GHz for phantom I, and cut-off frequency of 5 GHz for phantoms II and III).
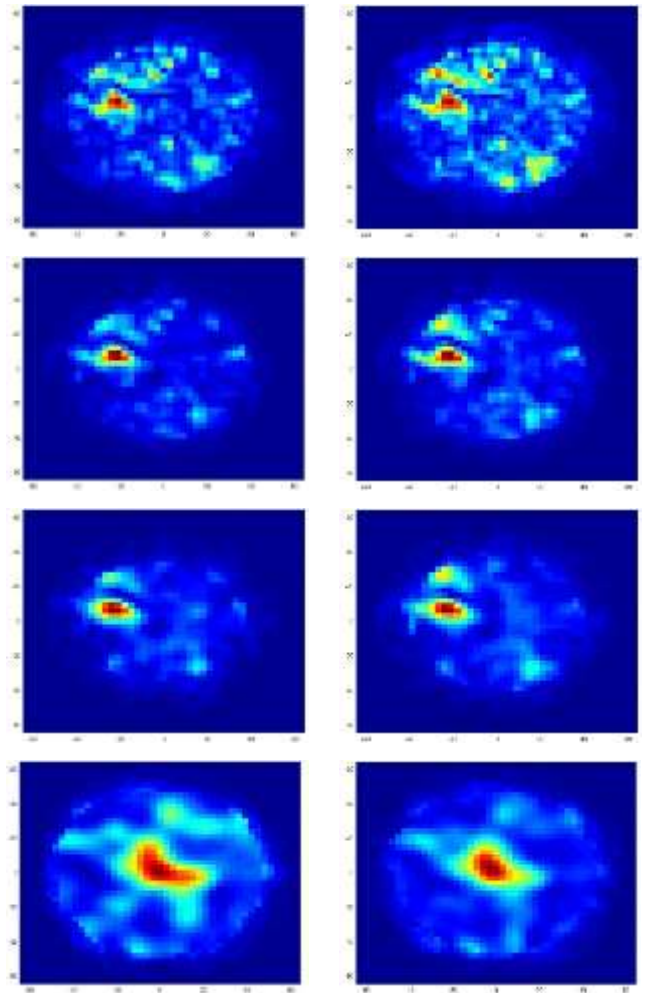

Fig. 3. Energy profile of breast phantom I. A Brickwall filter with a 4.5GHz cut-off frequency and a 20th order Butterworth filter with -3dB were used, left and right, respectively. From top to bottom: $d = 0$, $d = 1$ $d = 2$ and $d = 3$.

The resulting signal should have the skin response removed, but it will comprise the set of internal backscatterers and that set rotated by θ_{rot}.

B. Beamformer

Finally, a beamforming algorithm was applied to spatially focus the backscattered signals and create an energy profile of the breast phantom. High-energy regions identify the presence and location of significant dielectric scatterers which may represent breast tumours.

Computationally, the TD method requires the manipulation of large arrays to implement the time delays, whereas the FD method may be implemented using matrix multiplication, which is often a more efficient method especially when the time window T_w is relatively large (thus restricting the number of frequencies for which the phase needs to be computed).

Using the time delay theorem of the Fourier Transform, the total field reconstructed at point $\boldsymbol{\rho}$, in the FD, is:
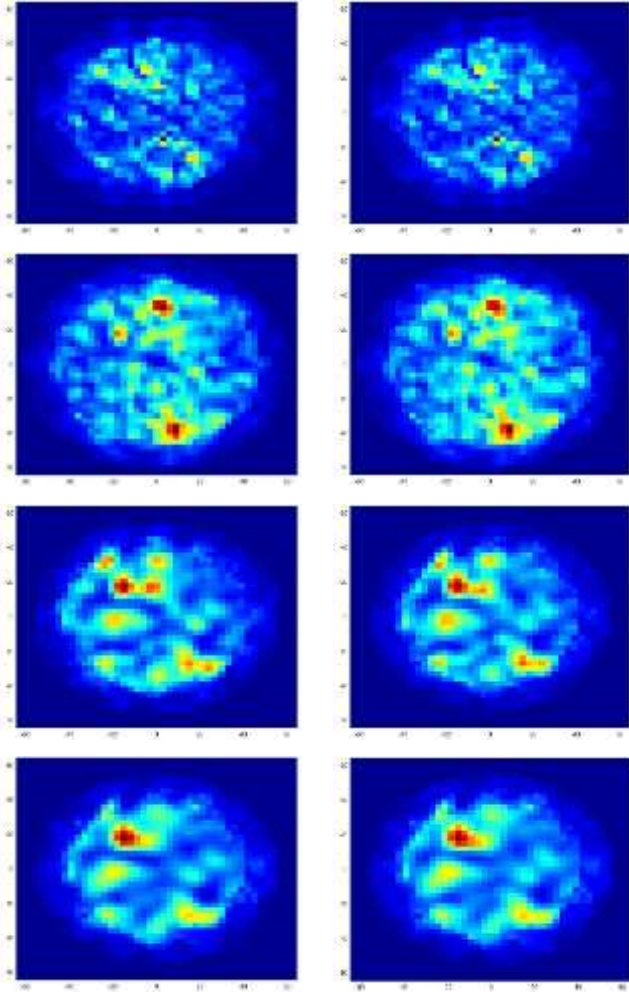or in terms of a summation over P discrete frequencies:

Fig. 4. Energy profile of breast phantom II. A Brickwall filter with a 5GHz cut-off frequency and a 20th order Butterworth filter with -3dB were used, left and right, respectively. From top to bottom: $d = 0$, $d = 1$ $d = 2$ and $d = 3$.

$$E_{\boldsymbol{\rho}}(m) = \sum_{n=1}^{N} \sum_{p=1}^{P} E_{nm}(f_P)e^{-j2\pi f_P \tau(\boldsymbol{\rho},\boldsymbol{\rho}_n)} \qquad (3)$$

where $\tau(\boldsymbol{\rho},\boldsymbol{\rho}_n)$ represents the delay from the point of interest to the receiver.

An intensity image may be created by calculating a normalised intensity at each point:

$$I_{\boldsymbol{\rho}}(m) = \sum_{m=1}^{M} |E_{\boldsymbol{\rho}}(m)|^2 \qquad (4)$$

The authors will examine the effects of the following filtering/compensation techniques:

- Distance correction: Equation 2 used in image reconstruction ignores wave attenuation. Spherical spreading of the signal due to lossy properties of biological tissue will be considered. However, early results suggest that a power law which compensates for spherical spreading is not necessarily the best, since there other causes of attenuation include scattering and the fact that nearby antennas are likely to have greater contamination from creep waves than signals which

have travelled further. A variable d will determine the influence of the distance correction in resulting energy profile of the breast phantoms: no scaling $d = 0$; linear scaling $d = 1$; quadratic scaling $d = 2$; and cubic scaling $d = 3$. The distance filter was implemented on the set of signals received, S, based on the transmitter-receiver distance such that:

$$S_{distance\_corrected}(n,m) = S(n,m) \times r_{nm}^d \qquad (5)$$

where $r_{mn} = |\rho_m - \rho_n|$ and r_{nm} is the matrix that stores the distances between antennas n and m, d is the distance variable which varies between 0 and 3.

$$E_{\boldsymbol{\rho}}(m,f) = \sum_{n=1}^{N} E_{nm}(f)e^{-j2\pi f\tau(\boldsymbol{\rho},\boldsymbol{\rho}_n)} \qquad (2)$$
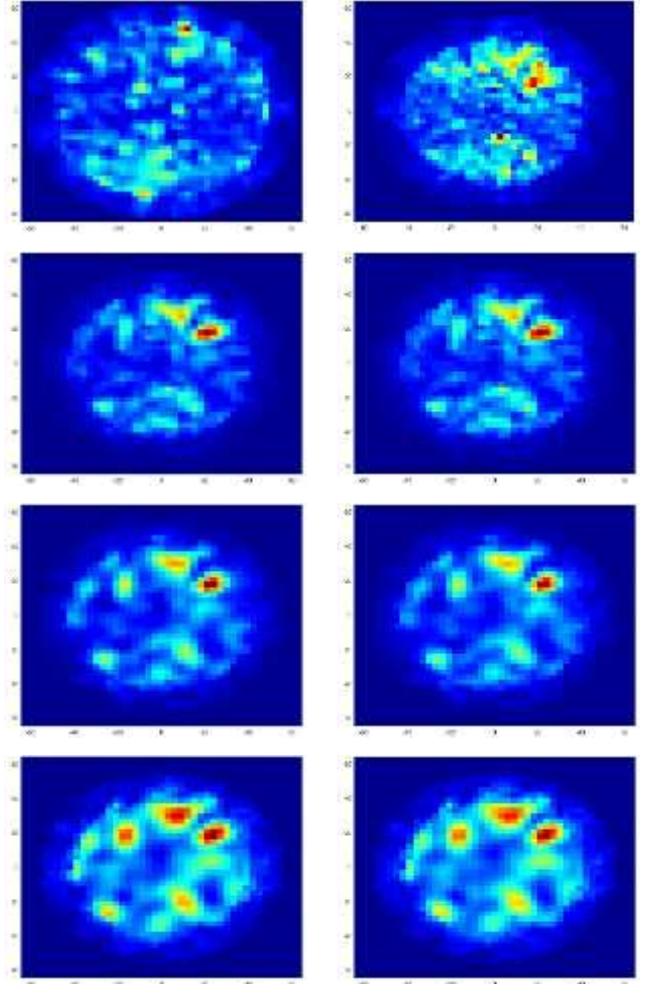

Fig. 5. Energy profile of breast phantom III. A Brickwall filter with a 5GHz cut-off frequency and a 20th order Butterworth filter with -3dB were used, left and right, respectively. From top to bottom: $d = 0$, $d = 1$ $d = 2$ and $d = 3$.

- Line of Sight Filter: only antennas with a direct line of sight to point $\boldsymbol{\rho}$ in the reconstruction of the image will be considered. An antenna at ρ_m with a cone of angle of θ_a,

and pointing in direction $\hat{r_m}$, where $\hat{r_m}$ is the unit vector in the direction of the radius at point ρ, is included in the calculation if:

$$\frac{\rho - \rho_m}{|\rho - \rho_m|} \cdot \hat{r_m} \leq \cos \theta_a \qquad (6)$$

- Spectral Filtering: a low pass Brickwall filter with cut-off frequencies of 4.5 and 5 GHz will be considered, as well as a 20th order Butterworth filter with -3dB (and comparable cut-off frequencies of 4.5 and 5 GHz). These frequencies were chosen after analysing the zero mean signal over all the antenna paths (Figure 2).

IV. RESULTS

The resulting energy profile of the breast phantoms when using the low pass Brickwall filter (with cut-off frequencies of 4.5 GHz for Phantom I, and cut-off frequencies of 5 GHz for Phantom II and III) and a 20th order Butterworth filter with -3dB (with equivalent cut-off frequencies of 4.5 GHz for Phantom I and 5 GHz for Phantoms II and III), with four distance corrections, are shown for the three phantoms I, II and III, in Figures 3, 4 and 5, respectively.

The tumour region in breast phantom I is correctly detected at its original location using both a Brickwall and a 20th order Butterworth filters, particularly with a distance correction factor $d=1$ and $d=2$.

The tumour region in breast phantom II is correctly detected at its original location using both a Brickwall and a 20th order Butterworth filters, particularly with a distance correction factor $d=2$. The fibroglandular region is also correctly detected with the same filters.

The tumour region in breast phantom III is harder to be correctly detected at its location with both a Brickwall and a 20th order Butterworth filters. The fibroglandular region produces higher backscatter energy than the tumour region., but the tumour region is still noticeable with all the tested distance correction factors.

V. CONCLUSIONS

Tumours were detected in each of the tested scenarios and low pass Brickwall filters were easily implemented and led to faster processing times. Filter cut-off frequencies based on the spectra of the measurements need to be further investigated and tested in more imaging scenarios.

REFERENCES

[1] J. Bourqui *et al*, "A Prototype System for Measuring Microwave Frequency Reflections from the Breast," *International Journal of Biomedical Imaging,* vol. 2012, p. 12 pages, 2012.

[2] T. Henriksson *et al*, "Clinical Trials of a Multistatic UWB Radar for Breast Imaging," in *2011 Loughborough Antennas & Propagation Conference*, Loughborough, UK, 2011, pp. 1-4.